Special Issue: Continuous-Discontinuous Long Fiber-Reinforced Polymer Composite Structures

JOURNAL OF THERMOPLASTIC COMPOSITE MATERIALS

Journal of Thermoplastic Composite Materials
2025, Vol. 0(0) 1–25

DOI: 10.1177/08927057251331573
journals.sagepub.com/home/jtc
Sage

Formation and occurrence of subsurface damage mechanism with the analysis of optimal machining strategy when milling different fibre matrix combination of unidirectional FRP's

Felicitas Böhland[1], Remus Tutunea Fatan[2] and Volker Schulze[1]

Abstract

To utilise LFT (Long fibre thermoplastic) materials for structural components, they are reinforced with UD-tapes to achieve high stiffness and strength. Machining of unidirectional fibre reinforced plastics can cause various types of damage such as delamination, burrs or subsurface damage due to the anisotropy of the material and the resulting cutting conditions. A reduction of surface quality or component rejection can be the result. In addition to the usual process parameters such as feed rate the fibre type and the matrix material have a decisive effect on the separation mechanisms. In this paper different materials are analysed to provide a deeper understanding of the subsurface damage formation during the milling cut. The focus is on thermoplastic composites T700/PA6 and T700/PEEK as well as GF/PP and flax/PP. The composites with epoxy resin are reinforced with different carbon fibre types such as high tenancy (AS4), high modular (HM) and ultra-high modular (UHM) fibres. A spatially defined fibre cutting angle is used to analyse the subsurface damage area which varies due to uncut chip thickness, fibre type and matrix material. The damage range and depth is strongly influenced by the fibre type, as well as the fracture morphology due to bending induced fractures. Even for the flax/PP a

[1]Institute of Production Science (wbk), Karlsruher Institute of Technolgoy, Karlsruhe, Germany
[2]Department of Mechanical and Material Engineering, Western University, London, ON, Canada

Corresponding author:
Felicitas Böhland, Institute of Production Science (wbk), Karlsruher Institute of Technolgoy, Engelbert-Arnold-Str. 8, Kaiserstraße 12, 76131 Karlsruhe, Germany.
Email: felicitas.boehland@kit.edu

subsurface damage area can be observed, although their properties differ greatly. For T700/PA6 and T700/PEEK plastic deformation can be observed due to fibre-matrix fragments adhere back to the surface after cutting. The findings about the subsurface damage area are applied to the milling of an external radius. For UHM/epoxy there was no subsurface damage in milling an external radius. By using an optimised milling strategy the maximum damage depth can be reduced in T700/PA6 up to 26%, in HM/epoxy up to 52% and in AS4/epoxy up to 73%.

Keywords
FRP, surface analysis, subsurface damage, milling, fibre cutting angle, thermoplastic/thermoset

Introduction

Fibre reinforces composites (FRP) are widely used in aerospace, automotive and wind power industries due to beneficial properties such as high strength, stiffness and fatigue resistance.[1] Discontinuous long fibre reinforced polymer composites offer great design freedom and improved impact resistance, but only combined with unidirectional reinforcements such as UD-tapes the high stiffness and strength required for structural components can be achieved.[2] Although components are manufactured near-net-shape, some machining processes, such as milling and drilling, are necessary to achieve sufficient accuracy of the functional surfaces.[3] Due to the anisotropic structure of FRP's milling is challenging as different damage phenomena can occur depending on the fibre orientation.[4] These can be divided into top surface damage like delamination[5] and burrs[6] and subsurface damage like a saw-tooth profile and cavities.[7] Damage needs to be avoided as it can lead to costly rework, reduced performance or part rejection. The appropriate selection of tool geometry, cutting parameters like the fibre orientation and milling strategies is crucial to ensure the machining quality during the milling process.[8] As discontinuous long fibre reinforcement does not have the strength and stiffness of unidirectional fibre orientation the machinability also changes. While delamination can be controlled by appropriate cutting strategies such as milling with a twisted tool or tool inclination (see Figure 1), the subsurface damage does not have the same depth and extent of damage as with unidirectional reinforcements due to the microstructurally constantly changing fibre orientation. This means that unidirectional fibre reinforcements are more critical in terms of damage during milling, which is why they are the focus of this work.

In addition to classic parameters known from homogenous material, such as feed rate and cutting speed, the fibre cutting angle based on the unidirectional fibre direction is a critical factor.[8] In milling the fibre cutting angle changes due to the rotational movement of the cutting edge. Different definitions of the fibre cutting angle can be found in literature. Often it is determined two-dimensionally and defined as angle between the

cutting direction vector and the unseparated fibre in mathematically positive direction.[9] For spatial engagement conditions caused by inclination angles or a helix angle of the tool three-dimensional approaches are needed.[10] Therefore, the definition from Boehland et al.,[11] which is transferable to different spatial engagement milling situations, is applied in this study. Different fibre cutting angles θ_{ne} lead to different failure modes of the material and the resulting surface morphologies.[4] Two main failure phenomenon delamination and subsurface damage are discussed during milling (see Figure 2). If the fibre is inclined away from the cutting edge (θ_{ne} from $-90°$ to $0°$), local pressure peaks transverse to the fibre lead to breakage.[4] Hintze et al.[12] stated that this cutting condition can lead to delamination and burrs at the top layers during slot milling of unidirectional CFRP (see Figure 2(left)). Most researchers focus on this area and the resulting top layer delamination damage. The other less investigated area from $\theta_{ne} = 0°$ to $\theta_{ne} = 90°$ where subsurface damage occurs (Figure 2(right)) is also decisive for component quality. Under

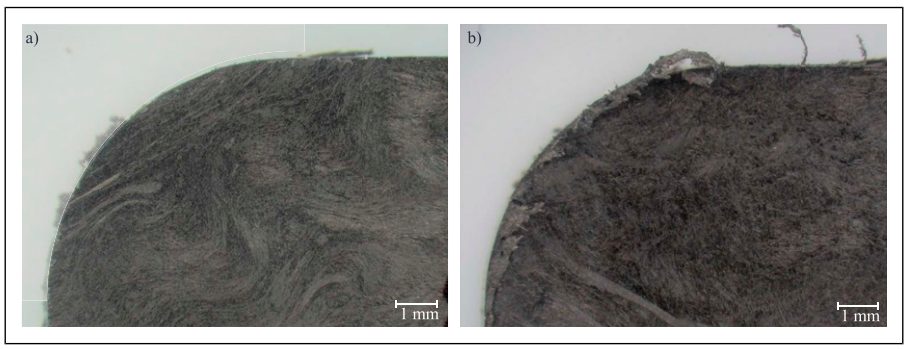

Figure 1. Delamination of LFT material milled with (a) tool inclination and twisted tool and (b) straight edge tool.

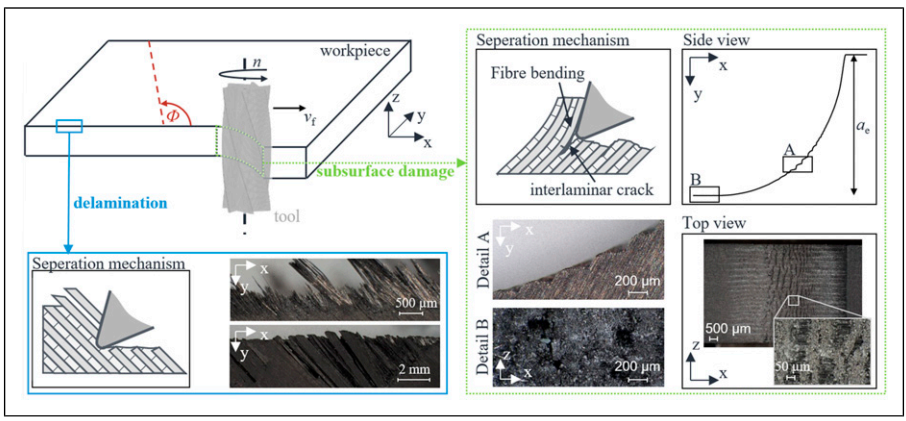

Figure 2. Damage mechanism (delamination and subsurface damage) due to milling.

unfavourable conditions it can lead to total failure of the component during cutting.[13] If the fibre is inclined towards the cutting edge, an increased bending load is applied to the material, leading to interfacial failure.[4] The subsurface damage is predominant in this fibre cutting angle range from 0–90°.[14] A strong deformation is triggered due to high bending load, resulting in fibre-matrix debonding along the fibre orientation. The crack spread in advance towards the cutting edge.[15] This often results in a so called saw-tooth profile (Figure 2(right) Detail A) observed by Heinrichs et al.[16] and surface cavities (Figure 2(right) Detail B).

Wang et al.[17] investigated the occurrence and formation mechanism of the surface cavity defects. The area of subsurface damage was limited to 50–60% of the region where the fibre is inclined towards the cutting edge. They showed at the surface that the saw-tooth profile at the surface is formed as a result of various fracture steps. First a fibre-matrix interfacial fracture is detected. Followed by bending induced fracture phenomenon. Then a second fibre-matrix fracture occurs, while the shear induced fractures represent the end. They also detected compression induced fibre fractures and fibre matrix debonding before the subsurface damage area and shear induced fibre fraction in combination with compression induced fracture occur afterwards. The fracture mechanism knowledge from Wang et al.[17] is mainly based on findings from bending, compression and tensile tests of single carbon fibres.[18,19] A study by Tanaka et al. was able to demonstrate the influence of the origin, i.e. pitch or pan based carbon fibres, on the fracture morphology in tensile and bending tests of single fibres.[20] Boehland et al.[11] expanded the findings of the subsurface damage area detected by Wan et al.[17] by stating that the subsurface damage area differs depending on the tool. They also detected the influence of chip thickness, rake angle, fibre cutting angle and the cutting edge rounding on saw-tooth profile dimension and occurrence in peripheral milling. In general the depth increases with rake angle and chip thickness and decreases with fibre cutting angle. In addition, the cutting edge has an optimum rounding for a minimum saw-tooth profile. The influence of the cutting edge rounding on the saw-tooth profile is also shown in Peter et al.,[21] where the rounding leads to a higher smearing of the matrix, especially in the saw-tooth valleys.

In almost all of these studies different carbon fibre types such as UHM-fibre (Dialed K63712),[21] IMA-fibre,[16] T300-fibre,[17] T800-fibre[13] and AS4-fibre[11] are used. While the general failure mechanisms are the same[22] the mechanical properties of the used fibre type can influence the extent of damage. Few studies have so far shown the effect of the fibre type on the machining performance: In the study of An et al[23] two carbon fibres (T800 and T700) were compared in terms of force and energy in the orthogonal cut. The composite with T800 always had a higher cutting force and specific cutting energy then T700. No statements about the resulting damage were made. There is evidence from modelling delamination using a minimum fibre radius that different carbon fibre types affect the delamination area.[24] A study of helical milling showed that carbon fibre reinforced material results in more burrs than glass fibre reinforced.[25] In addition to the fibre type, the bonding of fibre and matrix plays an important role in the machining process. Compared to conventional thermoset resigns thermoplastic ones offer the advantages of reparability and recyclability, which is why they will be used more in the future.[26] Comparing the

machining performance of thermoset (epoxy) and thermoplastic (PEKK) Ge et al.[27] found significantly distinct machining behaviour during drilling process. Under the same parameters CF/PEKK showed higher forces but lower delamination damage due to better interlaminar fracture toughness of CF/PEKK. The material removal is dominated by plastic deformation in CF/PEKK while brittle fracture is shown in CF/epoxy. Xu et al[28] evaluated the drilling performance of thermoplastic CF/PI and thermoset CF/epoxy and concluded that CF/epoxy performed with higher thrust force, higher cutting temperature and lower hole dimensional accuracy. Hocheng and Puw[29] showed that thermoplastic CF/ABS produces longer continuous chip and better surface quality than thermoset CF/epoxy. Liu et al.[30] compared a thermoset CF/epoxy and a thermoplastic CF/PEEK composite with the same fibre during milling. The thermoplastic shows better machining quality although the forces were higher and more compact interface bonding with the fibre was detected at the CF/PEEK. In addition, the residual tensile strength was higher with the thermoplastic resign. In addition Liu et al.[30] observed the temperature at the surface. For both materials the temperature decrease with increasing feed rate and increases with higher cutting speed.

To date, most comparisons of different FRP materials have been analysed in drilling. Especially comparing machining performance of thermoplastic and thermoset composites. However, the damage phenomena cannot be fully transferred to milling due to interrupted cut with changing local cutting conditions and different force load directions. As the damage caused during milling can affect the resulting surface it is important to analyse what happens during the cut. The orthogonal cut is usually used for this purpose, but it does not involve changing cutting conditions as in milling. Therefore the method developed in Boehland et al.[11] to analyse one cut during milling is used here. The aim of the study is to gain a deeper understanding of the damage phenomena due to different mechanical properties of composite combinations and the local cutting conditions.

In the following, the work first discusses the materials used, the experimental setup and the evaluation methods. For the initial sections, one milling cut is considered. The results are first analysed for occurring subsurface damage and depth based on fibre properties. The fracture mechanisms of the fibres are as well considered in this section. The influence of the matrix material on the separation mechanisms is taken into account in the next section. Subsequently, the effect of the different materials on the wear of the cutting edge is considered. Local process parameters, such as chip thickness, are important for milling and therefore their effect is analysed in the next section. Among other things, the actual chip thickness due to the damage depth is calculated. In the last section, an external radius will be milled. Based on the findings from one cut, the results will be interpreted. The milling path takes place in up and down milling. An optimised strategy combining up and down milling reduces subsurface damage.

Material, tool and experimental setup

The processed materials are unidirectional fibre reinforced plastics, and the specific properties are listed in Table 1. The properties of the resin materials in general are shown

Table 1 Properties of unidirectional laminates.

	Material thickness in mm	Fibre type	Filament diameter in μm	Fibre volume fraction	Fibre tensile modulus (GPa)	Fibre tensile strength (MPa)	Elongation at break	Manufacurer
UHM/Epoxy	3	Dialed K63716*[1]	11*[2]	60*[1]	640*[1]	2600*[1]	0,4*[2]	Haufler Composites
HM/Epoxy	3	Profil HR40*[1]	6*[2]	62*[1]	375*[1]	4410*[1]	1,1*[1]	Haufler Composites
AS4/Epoxy	3	AS4*[1]	7,1*[2]	60*1	231*[2]	4400*[2]	1,8*[2]	Haufler Composites
T700/PEEK	3	T700*[1]	7*[2]	60*[1]	230*[2]	4900*[2]	2,1*[2]	Haufler Composites
AS4/PEEK	6	AS4*1	7,1*[2]	60*[1]	231*[2]	4400*[2]	1,8*[2]	Haufler Composites
T700/PA6	3	T700*[1]	7*[2]	55*[1]	230*[2]	4900*[2]	2,1*[2]	Haufler Composites
HT/PA6	6	–	7[1]	52*[1]	234*[2]	3400[1]	1,4[1]	BUEFA Thermoplastic Composites
GF/PP	3	–	4–24[1]	46*[1]	~74*[4]	3400[1]	3,5–4[1]	BUEFA Thermoplastic Composites
flax/PP	6	–	5–38[31]	50*[1]	~31*[4]	800–1500[32]	~2*[1]	BUEFA Thermoplastic Composites

*1data from composite manufacturer, *2data sheet from fibre manufacturer,*4calculated by data sheet UD-tape: $E_{fibre} = (E_{UD\text{-}tape} - + E_{matrix}*(1\text{-}v_{fibre}))/v_{fibre}$.

Table 2. Properties of resin materials.[1,33]

	Tensile modulus in GPa	Tensile strength in MPa	Elongation in %	Tg in °C	Ts in °C
Epoxy	2.8–3.4	40–75	1.3–5	80–120	
PEEK	3.5–3.8	90–105	>50	140–145	340
PA6	3.0–3.5	75–100	>20	47–80	265
PP	1.3–1.8	30–40	>50	−27	163–176

in Table 2. Different fibre types and matrix material are investigated to examine the influence of the material combinations on the damage phenomena during milling.

The fibre orientation angle Φ defines the global fibre direction (see Figure 3(b)). The fibre orientation is varied to obtain same local fibre cutting angles at different theoretic uncut chip thicknesses. All tests are carried out with a polycrystalline diamond (PCD), single edge tool. The diameter is 12 mm and the helix angle is 2°. The rake angle is 0°, while the clearance angle is 5°.

All peripheral milling experiments are performed on a Heller MC16 machining centre without coolant and were repeated at least 2 times. The schematic experimental setup is shown in Figure 3(a). A pre-cut is made before the measuring cut to create standardised conditions for each experiment. The cutting parameters for the pre-cut are a cutting speed v_c of 100 m/min, a feed per tooth f_z of 0.125 mm and a radial depth of cut a_e of 0.2 mm. Different milling strategies were applied, all with a rapid traverse movement 135° to the feed direction which takes place before the milling tool has reached the end of the specimen (see Figure 3(c1)). This means that the surface during one single milling cut remain intact and can be analysed in detail. The experiments are divided into the milling strategy of a straight edge, in which quasi constant fibre cutting angles are set (CFCA) and is represented in Figure 3(c1). Secondly, milling an external radius of r = 6 mm, which leads to variable fibre cutting angles (VFCA) over the cutting path, see Figure 3(c2)/(c3). The milling of the external radius is also used for the optimised milling strategy where combination of up and down-milling is used. Until a defined angle φ up milling is used and afterwards until the same angle down milling to reduce damage (see Figure 3(c4)).

While the CFCA is carried out with the fibre orientations 60°, 80° and 100° for all materials, the milling of VFCA is performed with 10° and all materials with 3 mm material thickness. The fibre orientation of 10° leads to an external radius that passes through the same fibre cutting angle range as is passed through during one milling cut at fibre orientation 80°. A large infeed a_e of 5.9 mm is selected to achieve a wide fibre cutting angle range across one single cut. This also means that the maximum uncut chip thickness almost corresponds to the feed per tooth f_z at the tool entry point. By the exit point it drops to zero. In up milling it is the other way around. While for the fibre orientation of 60° only a feed rate f_z = 0.065 mm/tooth, all the others were tested with all feed rates. The parameters used are listed in Table 3. To reduce the entry frequency and to get good force signals, tools with one cutting edge and a cutting speed of 50 m/min were selected to operate well below all eigenfrequencies. The force measurements are recorded using a three-component dynamometer (Kistler Type 9255C). The signals are sampled with 10 kHz and a low-pass filter with 3 kHz is applied to reduce signal noise.

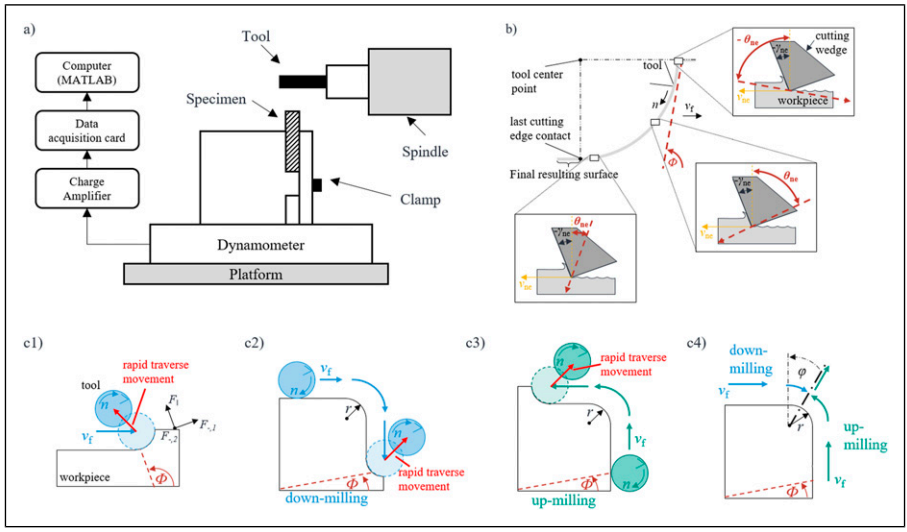

Figure 3. Experimental procedure with (a) schematic illustration of setup in Heller MC 16, (b) definition of fibre cutting angle and (c) cutting paths for variable fibre cutting angles (VFCA) in down- (c1) and up-milling (c2).

Table 3. Process parameter.

Milling type	Down and up milling
Cutting speed v_c in m/min	50
Feed per tooth f_z in mm/tooth	0.03, 0.065, 0.1
Radial depth of cut a_e in mm	5.9
Fiber orientation Φ in °	10, 60, 80, 100

Evaluation methods

The evaluation methods correspond to a previous own study, the key points are summarised here again. Detailed information can be found in Boehland et al.[11] To evaluate the local cutting parameters a dexel based geometric penetration simulation is used. For each discrete kinematic position (rotation angle of the tool), the penetration of the workpiece by the tool along the tool contour normal and thus the local chip thickness of the undeformed chip can be calculated (ISO 3002-1: 1982-08). According to the ISO 3002-1: 1982-08 the effective speed is vectorially decomposed in lateral and normal effective speed (v_{ne}). This normal effective speed is the basis of the used fibre cutting angle (θ_{ne}), which is defined analogous to the normal rake angle (see Figure 3(b)). This leads to a local fibre orientation relative to the cutting edge with reference to the normal speed, which can be transferred to a 3D situation. Both the force and the surface measurements are coupled with the simulation. For a straight cutting path, the force signal of a typical cut can be evaluated as time synchronous average over the cutting path. For this purpose, 80% of the total force

signal is used, to exclude transient phenomena when entering the sample. Additionally, local measurement errors are eliminated. This is not possible for milling the external radius, as the local fibre cutting angles change in each cut. Therefore, unaveraged force signals are used for these tests. The measured forces are analysed in the workpiece system (see x, y and z in Figure 2) and the resulting force is divided into forces transverse and parallel to the fibre. The force parallel to the fibre ($F_{\parallel}$) is defined along the fibre orientation and the positive direction points away from the final workpiece surface (Figure 3(c)). The first transverse force direction is in the laminate plane ($F_{\perp,1}$) while the second transverse force ($F_{\perp,2}$) is orthogonal to the laminate plane. It is important to note that the evaluation in directions at one time can be done. However, due to the 2° helix angle, the cutting edge is at different angles of rotation at one time step. And therefore at different local cutting conditions.

With a MarSurf XCR 20 roughness and contour measuring device the surface is captured via tactile profile method. To obtain more detailed measurements and thus validate the tactile method one measurement of each specimen of the CFCA strategy is recorded optically with the Sensorfar S neox. The roughness parameters S_a (mean arithmetic height) and S_z (maximal height) are calculated from the optical and tactical measurements using MATLAB in accordance with ISO 25187-2:2021-12. While the optical measurements were carried out with a resolution of 12 µm, the measuring distance for tactile measurements was 1 µm and the measuring speed was 0.2 mm/s. 50 lines are measured parallel to the feed direction, resulting in a distance of 0.1 mm at 6 mm material thickness and 0.05 mm between the lines at 3 mm. The obtained surface plots S_a are represented in Figure 4. The subsurface damage can be detected by an increase in the S_a values over the surface from one milling cut. While the depth of damage causally influences the level of S_a values. Exact values for the beginning and end of subsurface damage can be freely selectable according to requirements limit of S_a. In Boehland et al.[11] that limit was set to 4 µm. It can be seen that the damage areas are located at the same fibre cutting angles. And the detected beginning and end of the area, determined by the intersection of the mean S_a with the limit line at 4 µm, are almost the same. The extent of the damage differs, but only by low extent. The optical measurements showed a lower maximum S_a. This suggests that optical recording is probably no longer complete in the deepest damage depth valleys. Nevertheless, the optical measurement proofed the findings that the evaluation method used in the study Boehland et al.[11] is valid to detect the sub-surface damage.

Additionally, a REM (JEOL JSM-6010PLUS LW) was used to examine the formation of the saw-tooth profile in detail and analyse the fracture characteristic. Prior to REM observation, the samples were sputter coated with gold.

Furthermore, the structure of the machined surface is analysed by microscope images with Keyence VHX-970f. The same microscope is used to observe the wear of the cutting edge after each sample. The wear is characterized according to Denkena[34] by the cutting edge rounding r_β, the clearance flank wear S_α and the rake flank wear S_γ.

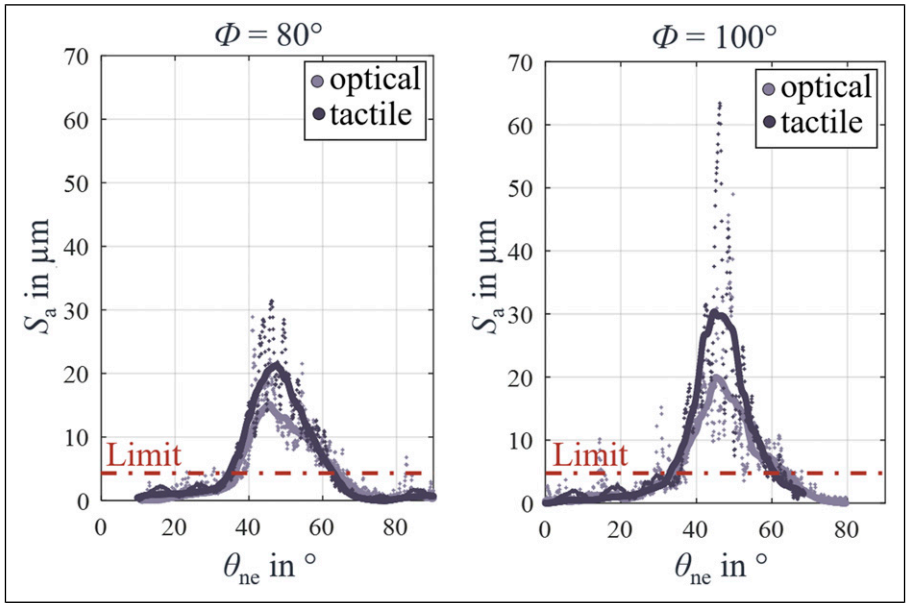

Figure 4. Detected subsurface damage areas with S_a via tactile and optical method at different Φ.

Results and discussion

Influence of fibre type

Comparing AS4/PEEK and T700/PEEK they only differ in material thickness and tensile strength. It is noticeable that the subsurface damage area and thus the saw-tooth formation are almost the same. The area is measured and defined by the mean S_a and the limit (presented in the evaluation methods). This means that the small difference in tensile strength of 500 MPa and the material thickness has minor influence on S_a and therefore the subsurface damage area (see Figure 5(d)–(f)). This can be also proofed by the fibres with the resin PA6. They slightly differ in the mechanical properties and insignificantly differ in subsurface damage area. The subsurface damage seems to be independent from the composite thickness, since AS4/PEEK with a thickness of 6 mm exhibits the same trend for S_a as the materials with 3 mm.

The fibres with clearly differing mechanical properties show that the subsurface damage area as well as the depth of the damage changes (see Figure 5(a)–(c)). The time at which the elongation at break of the fibre is reached is decisive for the depth of damage. This is the moment at which the maximum elongation is exceeded by the bending of the fibre. The formula to determine the minimal fibre bending radius r_{min_f} for sheet metal forming[35] can be used to view the trends. Hintze et al.[24] already used that formula for modelling delamination and showed good correlation. By knowing the elongation at break and the fibre diameter, a statement can be made about the tendency of the depth of subsurface damage. The correlation between r_{min_f} and S_z can be seen in Table 4. However, since only a slight deviation from S_a can be detected in materials with different resin but similar fibre properties,

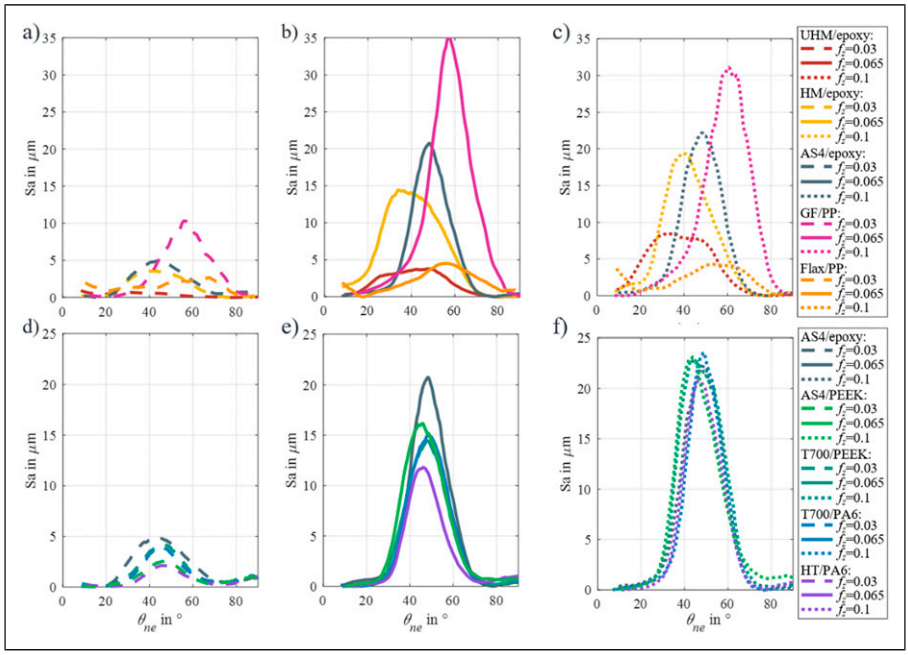

Figure 5. S_a due to different materials and feed per tooth with $\Phi = 80°$, (a) and (d) $f_z = 0.03$ mm/tooth, (b) and (e) $f_z = 0.065$ mm/tooth, (c) and (f) $f_z = 0.1$ mm/tooth.

this simplification is valid for the subsurface damage phenomenon. The influence of the fibre with its properties clearly dominates here. This makes it possible to estimate the depth of damage with a few mechanical parameters. In detail the damage depth depends on further influencing factors. On the one hand, mechanical properties such as the bonding between fibre and resin, the strength of the material supporting against bending and also the phenomenon of fibre bridging. On the other hand, process parameters such as cutting edge rounding, chip thickness and fibre cutting angle. Some of the factors are analysed in the following. Also the influencing factors interact with each other.

$$r_{\min\_f} = \frac{1}{2} * \left(\frac{1}{\varepsilon_B} - 1 \right) * d_f \tag{1}$$

The higher the minimal bending radius the earlier the fibres break and therefore the less deep the saw tooth profile and therefore S_z is. For the glass and flax fibre, the radius is a mean value as the fibre radii vary way more than with carbon fibres.

The influence of the mechanical properties of the fibre type is not only reflected in the damage depth, but also in the mechanism by which the fibre start and end to bend to such an extent that surface cavities or saw-teeth form due to the interlaminar crack between

fibre and matrix. Before the subsurface damage area begins, the fibres break mainly compression induced. When the saw-teeth appear, the bend and shear induced fibre fractures occur. The fibre cutting angle changes from large to small positive values during the cut resulting in increased bending load as θ_{ne} decreases, while the compressive load decreases (see Figure 6). The earliest beginning of subsurface damage is seen in the glass fibre reinforced composites (Figure 5(a)–(c)). This means that at a large θ_{ne} of ~80°, the glass fibre already bends so much that the fibre breaks due to exceeding the elongation at break. Although the superposition of bending and compressive load on the other fibres like UHM and HM is equally, they still break compressive induced. This can be explained by more flexible properties and the higher compressive fracture strain of the glass fibre. In contrast a UHM fibre has a comparatively low compliance to bending as well as tension and compression, it fractures from the fibres listed here under compressive load at the lowest elongation. Therefore, the bending induced fractures occurs at smaller fibre cutting angles compared with the other fibres. The HM as well as the AS4 and T700 fibres arrange due to their properties in between. The flax fibre has a slightly higher bending strength compared to glass fibre which explains the later beginning of subsurface damage. Overall,

Table 4. Calculated r_{min_f} and measured averaged maximum S_z with f_z = 0.065 mm/tooth and Φ = 80°.

Fiber type	r_{min_f} in µm	Averaged max. S_z in µm
UHM	1370	45
HM	270	90
AS4	194	121
GF	146 (mean value)	193
Flax	527 (mean value)	69

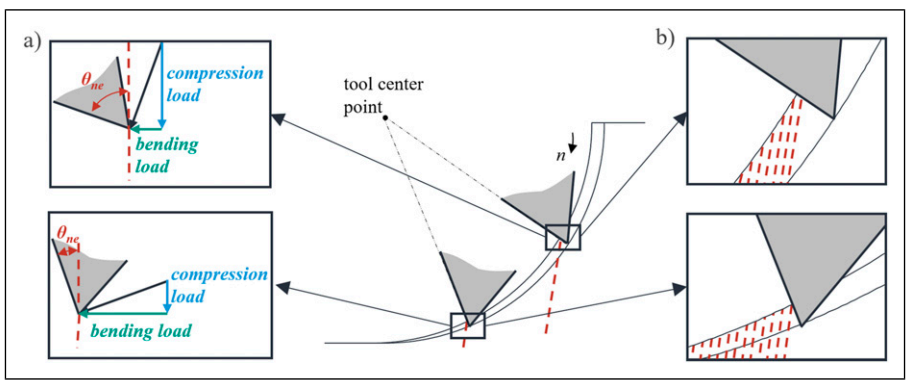

Figure 6. Influence of fibre cutting angle on milling situation due to (a) load situation and (b) supporting situation.

the more compliant and ductile the fibre the earlier, the more brittle and rigid the later the subsurface damage area begins.

With increasingly smaller θ_{ne} the separation mechanism changes to initially bending induced fractures without interfacial fibre-matrix debonding and then to compression and shear induced fractures. In addition, the load on the fibre is increasingly applied transversely to the fibre, what increases the influence of the tensile modulus in transverse fibre direction. The importance of the entire composite properties transverse to fibre direction, rises as individual fibres can no longer bend away easily due to the supporting effect of the composite fibres (see Figure 6(b)). As a result, fibre types such as glass fibres with quite as high modulus with and transverse to fibre direction have an earlier supporting effect against fibre-matrix debonding than carbon fibres, which have a pronounced transversal anisotopy in the fibre. This leads to an earlier end of the subsurface damage area (Figure 5(a)–(c)). Due to the combined effect of fibre thickness and fibre modulus on stiffness, the earlier end of the flax fibre is caused by the higher fibre thickness compared to the glass fibre. At the highest feed rate, the carbon fibres show the trend that the saw-tooth formation ends later with decreasing modulus transverse to the fibre direction. Nevertheless, at a feed rate of 0.065 mm/tooth, the UHM/epoxy subsurface damage ends earlier than the one of HM/epoxy. That shows the influence of the uncut chip thickness and its interaction with the influence of the mechanical properties.

Overall, an area of subsurface damage can be identified for all fibre types in the range of θ_{ne} from 0° to 90°. However, the exact appearance and depth of subsurface damage on the surfaces differ. In Figure 7 microscopic and surface plots of the surface roughness *(R)* are represented. In case of the glass fibre, the area is not only at a different position, but also differ in depth and wide. So just few saw teeth are formed. On the other hand, the UHM fibre, as mentioned above, breaks at much larger minimum bending radius. That forms many small saw tooth structures that do not form coherently across the material thickness. The surface with fibre T700 shows at the beginning of the subsurface damage area a similar behaviour. But from $\theta_{ne} \approx 50°$ the saw teeth become wider in feed direction and material thickness. Towards the end of the subsurface damage, less wide structures in material thickness direction can be seen again. The AS4 and the HM fibre are characterised by a similar course of the structure. The flax fibre shows the strongest deviating behaviour, although the roughness S_a increases significantly, no saw-tooth structure can be seen. Instead, there are isolated surface cavities. This is probably due to the natural origin of the flax fibre resulting in more varying single fibre properties of the composite. As a result, only few fibres will bend under the bend loading, while the others will resist at the same $\theta_{ne.}$

In Figure 8 the fibre fracture mechanism in the centre of the subsurface damage area are shown. The fibres T700, AS4 and the HM show the typical bending induced fractures that Wang et al.[17] have already shown in the subsurface damage area. They all exhibit a particulate or granular morphology as PAN based fibres do. The origin to produce the carbon fibre is decisive for the fracture morphology. This is why the UHM fibre, as a pitch-based carbon fibre, has a different rather sheet-like morphology. This is also known from tensile tests by Naito et al.[20] and is also reflected in the formation of the saw-tooth profile during milling. In addition, the UHM fibres sometimes break in themselves and

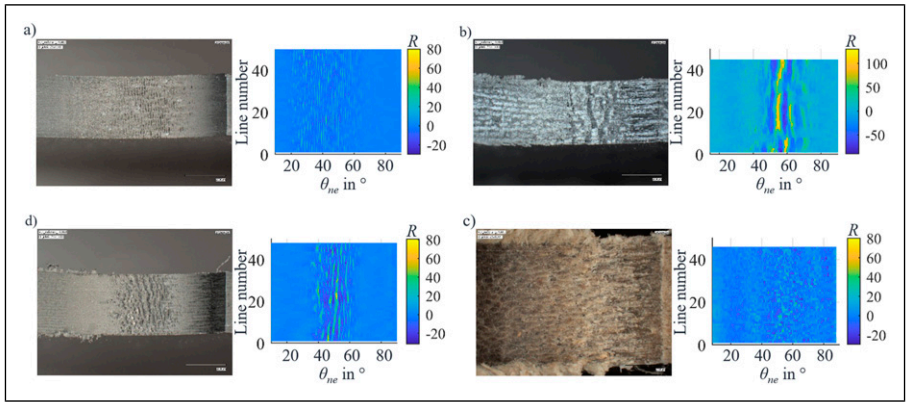

Figure 7. Microscopic images of surfaces during one cut and surface roughness with f_z = 0.065 mm/tooth and Φ = 80° with (a) UHM/epoxy, (b) GF/PP, (d) T700/PA6 and (c) flax/PP.

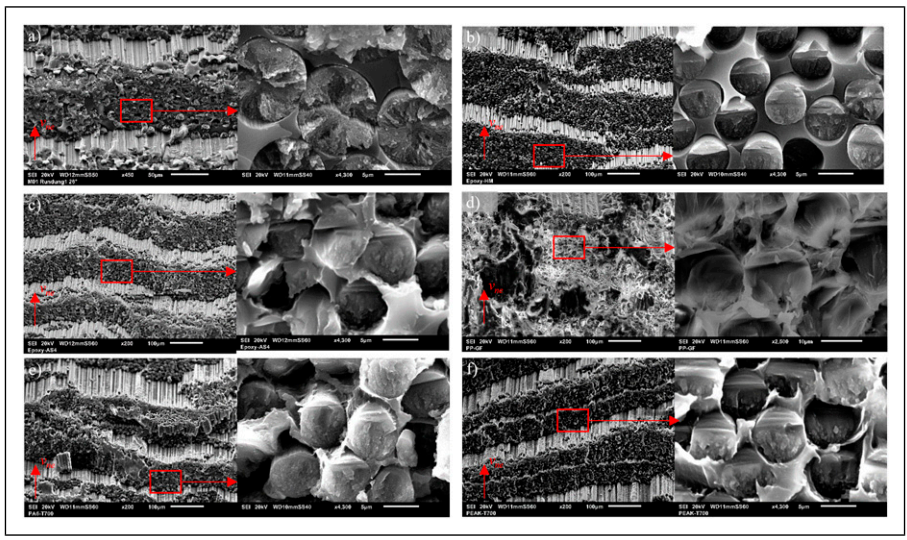

Figure 8. Saw-teeth structure and fracture morphology in the centre of the subsurface damage area for (a) UHM/epoxy, (b) HM/epoxy, (c) AS4/epoxy, (d) GF/PP, (e) T700/PA6 and (f) T700/PEEK.

steps are created within the fibre, see Figure 8(a). These arise transversely to the bending direction, i.e. in the same direction as the saw-teeth. This can be attributed to the brittle structure of the UHM fibre. The isotropic ductile glass fibre shows a particular granulate morphology under bending load. As for the PAN based carbon fibres a clear failure

initiation site on the tensile failure can be observed, but the surface is smoother. The compression side is smaller the lower the tensile modulus of the fibre.

The formation of the saw-teeth changes over one milling cut and therefore changing θ_{ne}. This can be observed for all materials. Figure 8 shows the resulting saw-tooth profile in the centre of the detected subsurface damage area, while Figure 9 shows the beginning a1–c1 and the end a2–c2 of the saw-tooth formation. At the beginning of the subsurface damage area, in the first step a fracture occurs along the fibre direction due to the bending load on the fibre. The different fractures are followed by bending induced fractured zone and a compression induced failure of the fibres. The compression induced failure zone is equivalent to the mechanism and surface that are apparent before the saw-tooth formation. This phenomenon occurs at large fibre cutting angles, where the cutting edge hits the fibre at a steeper angle. In the middle of the subsurface damage zone the procedure of saw-teeth formation is the same described by Wang et al.[17] First there is the same interfacial fracture followed by a bending induced fracture zone and a shear induced fracture zone. At the end of the saw-tooth formation the two zones get larger, and the interfacial fractures are less straight than in the middle zone. In Figure 9(a2)–(c2) a comb structure can be seen for UHM/epoxy, HM/epoxy and T700/PEEK. The initiation and progress of the interfacial fracture between fibre and matrix can be observed in Figure 9(c2). The debonding of fibre and matrix starts at one point and the crack propagation then runs through the material transverse to the feed direction.

Influence of matrix material

The matrix and fibre-matrix interaction has an influence on the mechanism of saw-tooth formation during milling. The interlaminar bonding between fibre and matrix and the mechanical properties of both play a decisive role. Figure 9(b1) shows that the HM fibre separate completely from the matrix due to the bending load. This means that there is no interlaminar crack in the matrix as often described in literature, but an interfacial fracture

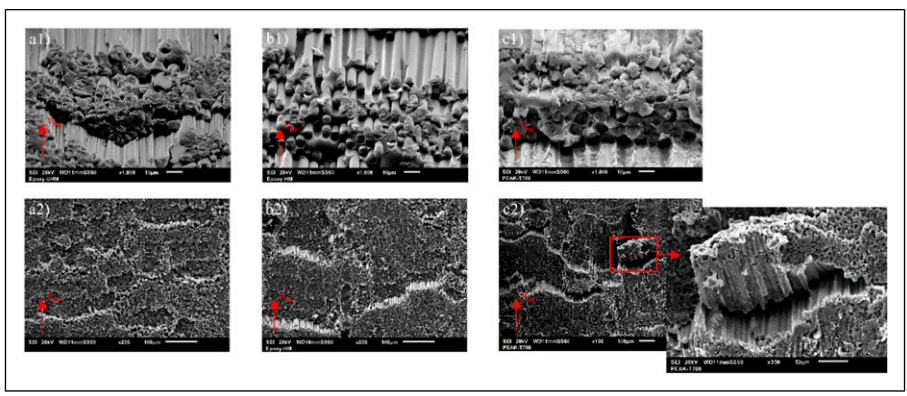

Figure 9. Beginning (a1–c1) and end (a2–c2) of the saw-teeth formation for (a) UHM/epoxy, (b) HM/epoxy and (c) T700/PEEK.

of fibre and resin. The fibre-matrix bonding is the weakest here, as there is a debonding of fibre and matrix in the zone where compression induced fractures are still present, although at shorter length. In case of T700/PEEK, the matrix is still visible through the fibres, indicating the plastic deformation of the resin during material debonding due to the bending load (Figure 9(c1)). The stronger bonding between fibre and matrix in thermoplastic described by Liu et al.[30] plays a decisive role in the formation of saw-teeth, especially for the fibre-matrix fracture. The brittle fibre in the UHM/epoxy means that there is no debonding of fibre and matrix, but rather a failure of the fibres in themselves. Figure 9(a1) shows that the fibres split along the fibre axis. The matrix is therefore not visible on the saw-tooth step as with the other fibres.

Due to the plastic formability of thermoplastics, another phenomenon occurs during the milling in the subsurface damage area that cannot be observed with epoxy. Figure 9(c2) and Figure 8(e) show how completely or partially separated chips are still bonded to the surface. This means that the heat input during machining causes an aggregation of the separated material fragments with the surface. In the subsequent cut, this means that the θ_{ne} cannot be clearly predicted. Figure 9(c2) shows that the fragments of fibre and matrix that were not completely separated were hit again by the cutting edge. This leads to cutting with negative θ_{ne} which leads to compression induces fractures transverse to the fibre length. The same phenomenon can also be observed with GF/PP, but is less pronounced. Therefore, it can clearly be attributed to composites with thermoplastics. The phenomenon occurs less around large θ_{ne}. But rather at the end of the subsurface damage area, which means at smaller fibre cutting angles.

Tool wear

The fibre-matrix combination also influence the wear of the cutting edge. The test for all materials were run in the same sequence and the development of the cutting edge for few materials is shown in Figure 10. If the development of the cutting edge rounding r_β is examined, it is noticeable that the brittle UHM fibre is less abrasive than the other fibre types (see Figure 10(a)). This means that the rounding remains almost constant for the considered cutting length. The rounding for the glass fibre has the highest scattering. Resulting in an inconstant rounding state over the material thickness. This can be attributed to the greater scattering of the fibre diameter. The Composite T700/PEEK shows a steeper increase in the clearance and rake face wear (Figure 10(b)). This increased abrasive wear on the rake and flank face could be due to the described adhesion of already separated material with the surface. As a result, more material needs to be machined under a wider spread of θ_{ne}, which leads to the abrasive effects. Flank and rake face wear is almost the same as the κ stays almost the same, see Figure 10(b).

The machining of AS4/epoxy led to a cutting edge breakage after a cutting length of approximately. 17 m. Particularly with a cutting edge that is sharp, the material combination lead to such a high load due to cutting in the damage area at maximum chip thickness that the cutting edge breaks. That does not happen with the thermoplastic composites T700/PA6 and T700/PEEK, although the fibre types behave similarly.

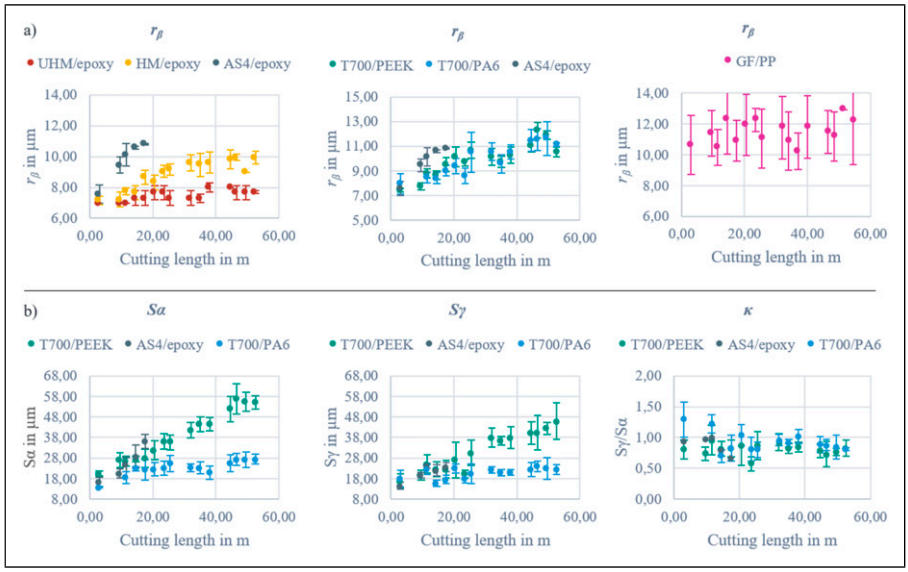

Figure 10. Cutting edge wear over the CFCA experiments measured with (a) r_β for different materials and (b) S_α, S_γ and κ for the materials T700/PEEK, T700/PA6 and AS4/epoxy.

The cutting edge rounding has an influence on the subsurface damage. Figure 11 shows mean S_a and S_z for various r_β. The influence on AS4/epoxy is greatest. An increase in r_β results in reduction of both mean S_a and maximum S_z (Figure 11(a)). The reduction is also present in UHM/epoxy and in T700/epoxy (Figure 11(b) and (d)), ableit to a lesser extent. The findings regarding AS4/epoxy confirm those from Boehland et al.[11] It was found there that the damage will increase again with further rounding. These levels of rounding were not reached in the study conducted here. For HM/epoxy from r_β = 8 µm to 13 µm both mean S_a and maximum S_z stays almost the same. In addition, there is the effect that from r_β = 13 µm to 18 µm, although mean S_a decreases slightly, the maximum S_z increases (Figure 11(c)). This shows that at certain condition of the damage, deeper saw teeth can be present, although the damage as a whole is decreasing. Compared to the influence of the fibre on subsurface damage, the influence of rounding is of little significance. The chip thickness, as described below, also can have greater influence.

Effect of the chip thickness

For all fibres, the uncut chip thickness has an additional influence on the damage depth. The smallest feed rate of 0.03 mm/tooth shows the lowest damage depth and area for all materials. Due to the high infeed a_e of almost the tool radius, the feed per tooth corresponds quasi to the maximum uncut chip thickness. Here the difference to 0.065 mm/tooth is greater than changing the feed from 0.065 to 0.1 (see Figure 5(a)–(c)). The fact that the cutting process almost takes place only in the cutting edge rounding changes the

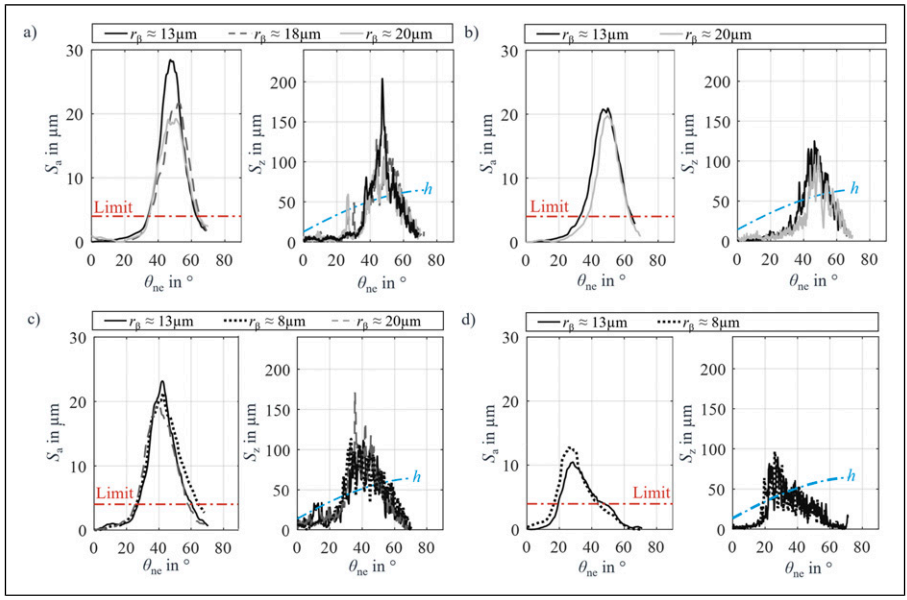

Figure 11. Influence cutting edge rounding on S_a and S_z for (a) AS4/epoxy, (b) T700/PA6, (c) HM/epoxy and (d) UHM/epoxy.

effective fibre cutting angle. Due to negative rake angles within the rounding a strong change of damage depth can be explained. The highest feed rate results in a further increase in depth of damage, except for AS4/epoxy and GF/PP. For these two materials there is a minimal reduction or no difference.

As already mentioned, the uncut chip thickness has a decisive influence on the subsurface damage area in addition to the mechanical properties. Figure 12(a) shows the damage depth as maximum S_z over the uncut chip thickness for UHM/epoxy, T700/PEEK and GF/PP. For all materials, the trend shows that damage depth decreases with smaller chip thicknesses. Damage no longer increases for a S_z above 0.06 mm. This means that the damage stagnates or even decreases (GF/PP). The damage depth with UHM/epoxy is at such low level with small chip thicknesses that a damage area can hardly be identified. Cutting with the edge rounding seems to lead to a change in cutting mechanism with no/fewer bending of the fibre.

It is important to note that the real uncut chip thickness (RUCT) in the subsurface damage area does not match the theoretical uncut chip thickness due to the saw-tooth profile created by previous cuts. The real chip thickness will therefore vary depending on the material and depth of damage. Figure 13 shows the real chip thickness plotted against the θ_{ne} and the material thickness. It was calculated from the theoretical uncut chip thickness minus the measured roughness. The white surfaces are such deep saw-tooth structures in which the cutting edge does not penetrate any material during the cut. This means that the greatest real chip thicknesses are achieved when machining UHM/epoxy

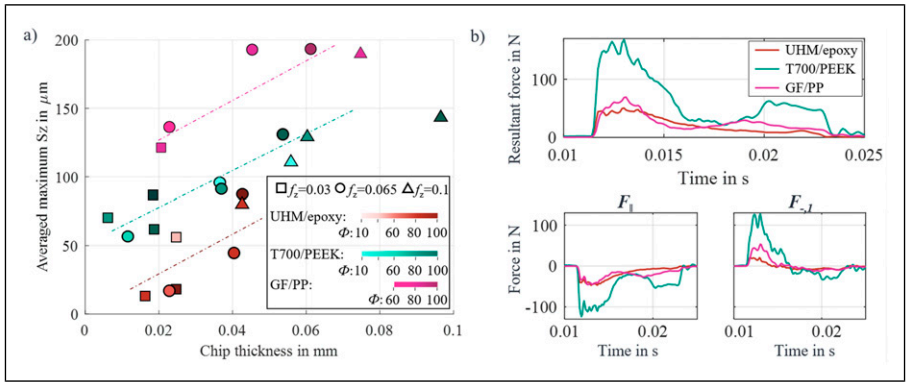

Figure 12. (a) Trend of averaged maximum S_z over uncut chip thickness and (b) cutting force progress over one tool rotation with f_z = 0.065 mm/tooth and Φ = 80°.

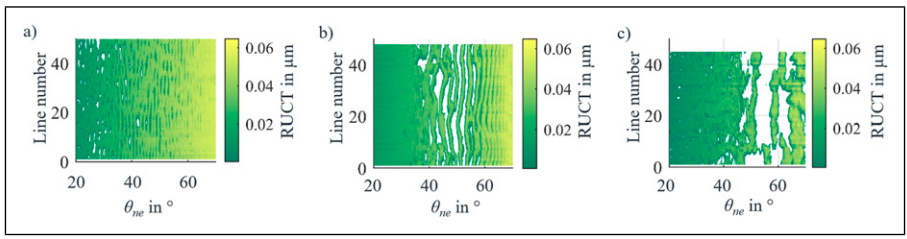

Figure 13. Real chip thickness of experiments with f_z = 0.065 mm/tooth and Φ = 80° of (a) UHM/epoxy, (b) T700/PEEK and (c) GF/PP.

with f_z = 0.065 mm/tooth and Φ = 80°. While the deepest damage processing GF/PP results in the largest areas without cutting material. Although the material UHM/epoxy has the greatest chip thickness the forces (see Figure 12(b)) are the lowest. This means the material is due to the brittle fibre and matrix less challenging to cut. The forces for T700/PEEK are the highest. This is consistent with the findings of Liu et al al[30] and can be explained by the strong bonding between fibre and matrix.

Milling an external radius

The examination of the external radius means that the final resulting surface and the corresponding fibre cutting angle at the created surface are analysed. As the external radius is processed, continuously changing θ_{ne} are traversed across one milling cut (see Figure 3(c1)/(c2). No two cuts are the same while milling the external radius. Figure 14 shows the subsurface damage of the external radius using S_a. With UHM/epoxy there is no subsurface damage area in either the up or down milling. This can be explained by the low depth of damage already detected at low uncut chip thicknesses. With each cut, the final

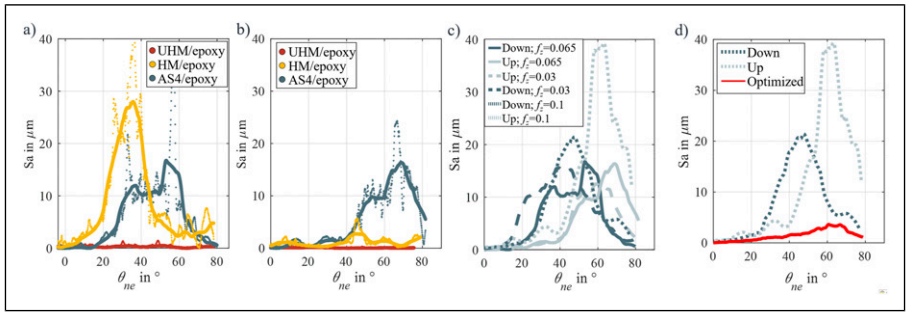

Figure 14. S_a of external radius for (a) down milling, (b) up milling with f_z = 0.065 mm/tooth and Φ = 10°, (c) up and down milling of AS4/epoxy and Φ = 10° and (d) milling strategies with f_z = 0.1 mm/tooth and Φ = 10°.

resulting surface is created with minimal chip thickness. The resulting damage area at the external radius of AS4/epoxy, as also described in Boehland et al,[11] differs depending on whether up or down milling takes place. This is because the deep damage that occurs during the cut can also affect the final surface. In up milling this leads to damage at fibre cutting angles that are larger than the largest detected during one cut. On the other hand, in down milling it leads to an expansion of the subsurface damage area to smaller fibre cutting angles. The HM/epoxy material shows slight damage in the up milling, while a higher amount of damage occurs in the down milling. When comparing different feed rates for AS4/epoxy, it is noticeable that the maximum damage depth increases with the feed rate. This applies to both the up and down milling.

A low degree of damage depth in the up milling occurs not only with composite HM/epoxy. While the materials T700/PA6 and T700/PEEK are in a similar range as with AS4/epoxy when down milling, the behaviour changes in up milling (see Figure 15). The thermoplastic matrix means that the detected damage range is comparatively low in the up milling (see Figure 15(b2)). This phenomenon also occurs for the thermoplastic GF/PP. The cutting edge entry at low uncut chip thicknesses leads to little or no damage. Since, as already mentioned, the thermoplastics have a better fibre matrix bonding, this could mean that this property becomes important at low chip thicknesses. In addition, in up milling a higher support effect occurs against the bending of fibres. Another reason could be that the thermoplastic deforms plastically, which could lead to a surface re-fusion that closes damage structures. However, the minor damage always occurs in the same area as with AS4/epoxy.

If the areas of damage in up and down milling are known, an optimisation can be carried out. By using the intersection point of the roughness curves (S_a.or S_z) the angle at which the milling strategy should be changed can be determined. The angle thus separates the sample into an area that is machined in up milling and on that is machined in down milling (see Table 5). Not only subsurface damage area can be minimised (see Figure 14(d)), but also the average S_z over the entire external radius and the maximum S_z (Table 5). This also applies to materials that show only minor damage in the up milling.

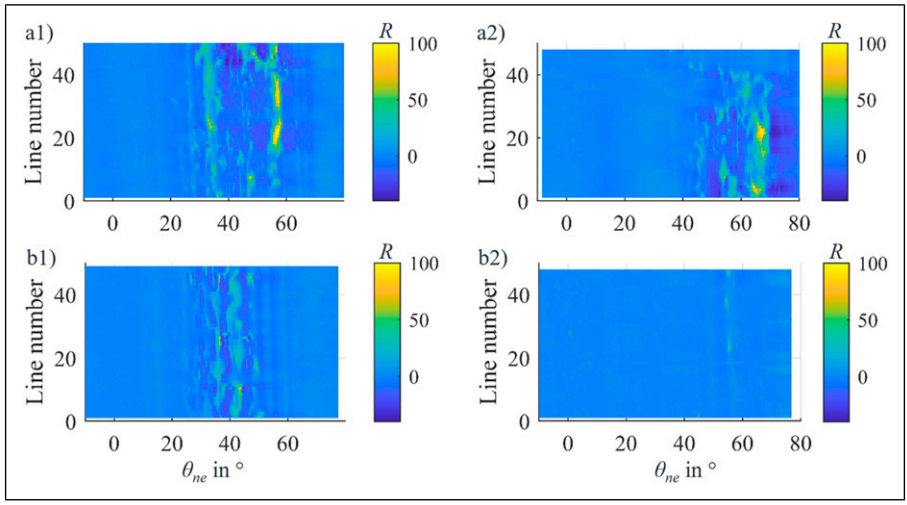

Figure 15. Surface roughness of (a) AS4/epoxy and (b) T700/PA6 in (a1/b1) down milling and (a2/b2) up milling with *fz* = 0.065 mm/tooth and Φ = 10°.

Table 5. Mean and max S_z for different materials in up, down and optimised milling strategy and optimised φ value.

	HM/epoxy; f_z = 0.1		T700/PA6; f_z = 0.065		T700/PA6; f_z = 0.1		AS4/epoxy; f_z = 0.065		AS4/epoxy; f_z = 0.1	
φ (optimised)	55°		26°		31°		10°		27°	
	Mean S_z	Max S_z	Mean S_z	Max S_z	Mean S_z	Max S_z	Mean S_z	Max S_z	Mean S_z	Max S_z
Optimised	5.6	12.8	5.1	26.2	6.1	23.9	19.4	98.8	9.9	34.2
Up milled	11.2	37.9	7.2	46.2	7.7	32.4	24,8	120.1	28.4	152.8
Down milled	8.2	27.1	18.6	115.1	35.5	190.6	29.7	135.4	29.3	130.9

The maximum S_z can reduced in T700/PA6 around 26 %, while in HM/epoxy up to 52 % and in AS4/epoxy until 73%. The averaged S_z can be also minimised by the optimized milling strategy for all materials.

Conclusion

Extensive peripheral milling test were performed with different unidirectional FRP materials and evaluated based on simulation using the spatial fibre cutting angle θ_{ne} defined in the effective normal plane. Two different experimental setups were used to

analyse the surface. One milling with a rapid transverse movement (CFCA) to analyse the surface over on milling cut provides deep insides to the influencing factors like the fibre-matrix interaction and the chip thickness and the formation mechanism of the subsurface damage area. The other experimental setup was milling an external radius to transfer the knowledge and optimize the milling path due to subsurface damage areas.

- The area in which subsurface damage occurs during a cut is largely determined by the fibre in the composite, while the matrix plays a minor role.
- The subsurface damage depth is strongly determined by the fibre properties such as filament diameter and elongation to break. The minimum fibre bending radius, whose formula is known from sheet metal forming, can be used to view the trend for the maximum damage depth of different FRP's.
- The lower the uncut chip thickness the lower the damage depth for all materials. The actual chip thickness must be taken into account and varies depending on the material and saw-tooth shape.
- The fracture mechanism at saw-tooth formation changes during the cut. At the beginning there are compression-induced alternating with the bending induced fracture zones. Which then became bending and shear induced fracture zones in the centre. At the end the zones become larger and a comb-like structure is created.
- The fracture morphology of the bending induced fractures of individual fibres depends not only on the fibre type, but also on the origin during fibre production. The pitch-based UHM fibre breaks due to its brittle structure also into itself, in contrast to the PAN-based carbon fibres.
- The fibre-matrix bonding is strongest for the thermoplastic materials, which can be seen in the fibre-matrix debonding zones of the saw-teeth. The fibre in UHM/epoxy does not detach from the matrix but breaks along the fibre axis. In the HM/epoxy the fibre detaches completely from the epoxy matrix. Whereas with the T700/PEAK matrix material still adheres to the fibres to the plastic debonding.
- The plastic deformation of the thermoplastic can be observed by the fact that fibre-matrix fragments are adhere back to the surface after cutting. The tool cutting edge then hits arbitrary fibre cutting angles.
- The milling of UHM/epoxy hardly results in cutting edge rounding. With the T700/PEAK the highest clear and rake face wear occurs.
- With the exception of AS4/epoxy, milling the external radius results in less subsurface damage for almost all materials in up than in down milling. UHM/epoxy shows no longer a subsurface damage area in both up and down milling due to the low chip thicknesses at the resulting surface. Nevertheless a milling strategy that runs one part in up milling and the other in down milling can reduce the damage depth for all materials. The maximum damage depth is reduced by up to 26% with T700/PA6, 52% with HM/epoxy and up to 73% with AS4/epoxy.

A precise knowledge of the formation and occurrence of the subsurface damage area due to different fibre-matrix combinations makes it possible to avoid it or minimise the

damage by the optimized milling strategies. The simulation based spatial evaluation can be used to transfer the knowledge to complex tool geometries and process paths. Due to the development of fibres and matrices in terms of sustainability it is important to consider the influence on machining. In further work, it would be useful to measure the mechanical properties of the composites parallel to the machining experiments. This would allow a direct coupling and the inclusion of values such as the interfacial shear strength or the effect of fibre bridging could be included in the evaluation. Furthermore, other factors influencing the machining, such as temperature, especially at different cutting speeds and thus energy inputs, can be taken into account. Also the interaction of different materials with different tools should be considered.

Acknowledgments

The authors acknowledge gratefully the funding support of the German Research Foundation (DFG) within the International Research Training Group "Integrated engineering of continuous discontinuous long fiber reinforced polymer structures" (IRTG 2078). The authors acknowledge gratefully Evgueni Bordatchev and the National Research Council of Canada for providing the optical surface measurements.

Declaration of conflicting interests

The author(s) declared no potential conflicts of interest with respect to the research, authorship, and/or publication of this article.

Funding

The author(s) disclosed receipt of the following financial support for the research, authorship, and/or publication of this article: The research documented in this manuscript has been funded by the Deutsche Forschungsgemeinschaft (DFG, German Research Foundation), within the International Research Training Group "Integrated engineering of continuous-discontinuous long fiber reinforced polymer structures" (GRK 2078).

ORCID iDs

Felicitas Böhland https://orcid.org/0009-0009-3067-347X
Volker Schulze https://orcid.org/0000-0003-2428-4127

Data Availability Statement

Data will be made available on request.

References

1. Schürmann H. *Konstuieren mit Faser-Kunststoff-Verbunden*. Berlin, Heidelberg: Springer, 2007.
2. Böhlke T, Henning F, Hrymak A, et al. (eds) *Continuous–discontinuous fiber-reinforced polymers: an integrated engineering approach*. Munich, Germany: Carl Hanser Verlag, 2019.

3. Ehrenstein GW. *Faserverbund-Kunststoffe. Werkstoffe – Verarbeitung – Eigenschaften*. München: Hanser, 2006.
4. Rummenhöller S. *Werkstofforientierte Prozeßauslegung für das Fräsen kohlenstofffaserstärkte Kunststoffe*. Dissertation, Aachen, TH, 1996.
5. Colligan K and Ramulu M. Delamination in surface plies of graphite/epoxy caused by the edge trimming process. In: *Processing and manufacturing of composite materials*, 1991, p. 27.
6. Hocheng H, Puw H and Huang Y. Preliminary study on milling of unidirectional carbon fibre reinforced plastics. *Compos Manuf* 1993; 4: 103–108.
7. Haddad M, Zitoune R, Bougherara H, et al. Study of trimming damages of CFRP structures in function of the machining processes and their impact on the mechanical behavior. *Compos Part B Eng* 2014; 57: 136–143.
8. Schütte C. *Bohren und Hobeln von kohlenstofffaserverstärkten Kunststoffen unter besonderer Berücksichtigung der Schneide-Faser-Lage*, Dissertation, Hamburg, TU, 2014.
9. Hohensee V. *Umrissbearbeitung faserverstärkter Kunststoffe durch Fräsen und Laserschneiden*, Dissertation, Hannover Univ., Hanover, 1992.
10. Hintze W and Brügmann F. Influence of spatial tool inclination on delamination when milling CFRP. *J Mater Process Technol* 2018; 252: 830–837.
11. Boehland F, Hilligardt H and Schulze V. Analysis of subsurface damage during milling of CFRP due to spatial fibre cutting angle, tool geometry and cutting parameters. *Compos B Eng* 2024; 281: 111533.
12. Hintze W, Hartmann D and Schütte C. Occurrence and propagation of delamination during the machining of carbon fibre reinforced (CFRPs) – An experimental study. *Compos Sci Technol* 2011; 71: 1719–1726.
13. Liu C, Ren J, Shi K, et al. Investigation of fracture mechanism evolution model for UD-CFRP and MD-CFRP during the milling process. *Compos Struct* 2023; 306: 116585.
14. Wang XM and Zhang LC. An experimental investigation into the orthogonal cutting of unidirectional fibre reinforced plastics. *Int J Mach Tool Manufact* 2003; 43: 1015–1022.
15. Sheikh-Ahmad JY. *Machining of polymer composites*. New York, London: Springer, 2009.
16. Henerichs M, Voß R, Kuster F, et al. Machining of carbon fiber reinforced plastics: influence of tool geometry and fiber orientation. *CIRP J Manuf Sci Technol* 2015; 9: 136–145.
17. Wang C, Liu G, An Q, et al. Occurrence and formation mechanism of surface cavity defects during orthogonal milling of CFRP laminates. *Compos B Eng* 2017; 109: 10–22.
18. Silva JLG and Johnson DJ. Flexural studies of carbon fibres. *J Mater Sci* 1984; 19: 3201–3210.
19. Hawthorne H and Teghtsoonian E. Axial compression fracture in carbon fibres. *J Mater Sci* 1975; 10: 41–51.
20. Naito K, Tanaka Y, Yang J, et al. Flexural properties of PAN and pitch-based carbon fibers. *J Am Ceram Soc* 2009; 92: 186–192.
21. Peter M, Sauer K, Regel J, et al. Effects of orthogonal cutting with different cutting edge microgeometry on the surface integrity of unidirectional carbon fibre reinfored plastics. In: MIC procedia, 2022, pp. 080–087.
22. Slamani M and Chatelain J. A review on the machining of polymer composites reinforced with carbon (CFRP), glass (GFRP), and natural fibers (NFRP). *Discov Mechanical Engineering* 2023; 2: 387.

23. An Q, Ming W, Cai X, et al. Study on the cutting mechanics characteristics of high-strength UD-CFRP laminates based on orthogonal cutting method. *Compos Struct* 2015; 131: 374–383.
24. Hintze W and Hartmann D. Modeling of delamination during milling of unidirectional CFRP. *Procedia CIRP* 2013; 8: 444–449.
25. Pereszlai C, Geier N, Poór DI, et al. Drilling fibre reinforced polymer composites (CFRP and GFRP): an analysis of the cutting force of the tilted helical milling process. *Compos Struct* 2021; 262: 113646.
26. Rudolph N, Kiesel R and Aumnatea C. *Understanding plastics recycling: economic, ecological, and technical aspects of plastic waste handling*. 2nd ed. Munich, Germany: Hanser eLibrary, Hanser, 2020.
27. Ge J, Luo M, Zhang D, et al. Temperature field evolution and thermal-mechanical interaction induced damage in drilling of thermoplastic CF/PEKK – A comparative study with thermoset CF/epoxy. *J Manuf Process* 2023; 88: 167–183.
28. Xu J, Li C, Dang J, et al. A study on drilling high-strength CFRP laminates: frictional heat and cutting temperature. *Materials* 2018; 11: 2366.
29. Hocheng H and Puw HY. On drilling characteristics of fiber-reinforced thermoset and thermoplastics. *Int J Mach Tools Manuf* 1992; 32: 583–592.
30. Liu S, Zhang Z, Zhao J, et al. A comparative study on milling-induced damages and residual tensile strength during milling of thermoplastic and thermoset carbon fibre reinforced polymers. *Polym Test* 2023; 125: 108132.
31. Franck R. *Bast and other plant fibres, material science, agricultural and food science*, 2005.
32. Bos H, Van Den Oever M and Peters O. Tensile and compressive properties off flax fibres for natural fibre reinfoced. *Composites* 2002; 37: 1683–1692.
33. Neitzel M, Mitschang P and Breuer U. *Handbuch Verbundwerkstoffe*. Verlag: Carl Hanser Verlag GmbH & Co. KG, 2014.
34. Denkena B, Friemuth T, et al. *Kantenpräparation an Hartmetallwerzeugen*. VDI-Verlag: VDI-Z Spezial Werkzeuge, 2005, pp. 51–54.
35. Lange K. *Umformtechnik, Band 3: Blechbearbeitung*. Berlin Heidelberg: Springer Verlag, 1990.